ACS OMEGA

Open Access

http://pubs.acs.org/journal/acsodf

Article

Stearate-Coated Biogenic Calcium Carbonate from Waste Seashells: A Sustainable Plastic Filler

Maria Luisa Basile, Carla Triunfo, Stefanie Gärtner, Simona Fermani, Davide Laurenzi, Gabriele Maoloni, Martina Mazzon, Claudio Marzadori, Alessio Adamiano, Michele Iafisco, Devis Montroni, Jaime Gómez Morales, Helmut Cölfen, and Giuseppe Falini*

Cite This: *ACS Omega* 2024, 9, 11232−11242

Read Online

ACCESS | Metrics & More | Article Recommendations | Supporting Information

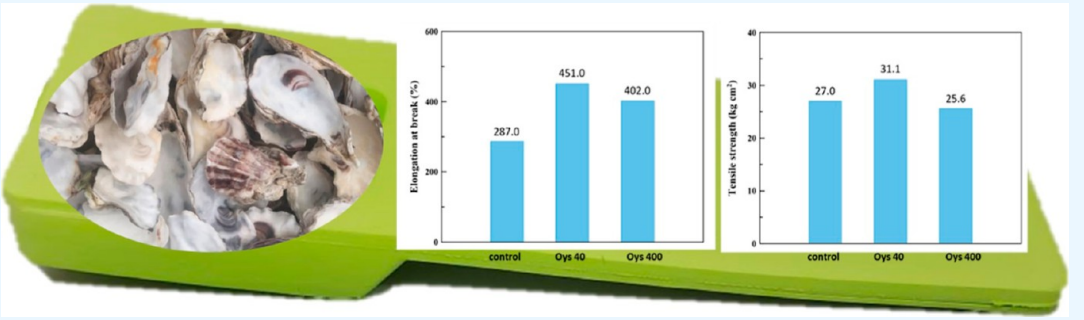

ABSTRACT: Waste seashells from aquaculture are a massive source of biogenic calcium carbonate (bCC) that can be a potential substitute for ground calcium carbonate and precipitated calcium carbonate. These last materials find several applications in industry after a surface coating with hydrophobic molecules, with stearate as the most used. Here, we investigate for the first time the capability of aqueous stearate dispersions to coat bCC powders from seashells of market-relevant mollusc aquaculture species, namely the oyster *Crassostrea gigas*, the scallop *Pecten jacobaeus*, and the clam *Chamelea gallina*. The chemical−physical features of bCC were extensively characterized by different analytical techniques. The results of stearate adsorption experiments showed that the oyster shell powder, which is the bCC with a higher content of the organic matrix, showed the highest adsorption capability (about 23 wt % compared to 10 wt % of geogenic calcite). These results agree with the mechanism proposed in the literature in which stearate adsorption mainly involves the formation of calcium stearate micelles in the dispersion before the physical adsorption. The coated bCC from oyster shells was also tested as fillers in an ethylene vinyl acetate compound used for the preparation of shoe soles. The obtained compound showed better mechanical performance than the one prepared using ground calcium. In conclusion, we can state that bCC can replace ground and precipitated calcium carbonate and has a higher stearate adsorbing capability. Moreover, they represent an environmentally friendly and sustainable source of calcium carbonate that organisms produce by high biological control over composition, polymorphism, and crystal texture. These features can be exploited for applications in fields where calcium carbonate with selected features is required.

INTRODUCTION

Calcium carbonate ($CaCO_3$) is one of the most widely used materials, having a sale of about 150 Mton per year.[1] It is commonly obtained by grinding the geogenic raw mineral, limestone, forming ground calcium carbonate mineral (GCC), or by carbonation of a calcium hydroxide slurry, generating the so-called precipitated calcium carbonate (PCC).[2] GCC is classified according to the size of the grains that have the shape of irregular rhombohedra. This material is made of calcite, the most thermodynamically stable $CaCO_3$ polymorph, and no chemical change is involved in its preparation process.[3] On the other hand, the manufacture of PCC requires more stages such as calcination, hydration/slacking, carbonation, filtration, and drying. The size and shape of PCC grains can be controlled, and impurities are removed during the synthetic process. PCC is generally obtained as rhombohedral or scalenohedral calcite, but aragonite and vaterite, the kinetically favored and the metastable $CaCO_3$ polymorph, respectively, can also be obtained.[2] In PCC, a rigorous $CaCO_3$ polymorphic selection is a difficult task, and often traces of other polymorphs coexist with the preponderant one. However, PCC particles are mostly uniform in size and regular in shape when compared to GCC.

Received: August 21, 2023
Revised: November 3, 2023
Accepted: November 8, 2023
Published: February 29, 2024

Thus, PCC is used in more advanced applications than those of GCC.[4,5]

$CaCO_3$ is also the main component of mollusc shells and other skeletal structures of many calcifying invertebrates, where it usually represents more than 95 wt %.[6−9] The $CaCO_3$ formed by organisms is obtained under accurate and faithful biological control. This implies, by example, that different species are able to form structures of aragonite, calcite, or with a precise spatial distribution of both polymorphs.[10] In the latter case, they are located in different layers and never mixed together.[7] In biogenic $CaCO_3$ (bCC), the crystalline texture and the presence of trace elements is species-specific.[8,11] This depends on the geochemical features of the living site of the calcifying organism and can be customized.[12] Thus, bCC offers controlled species- and site-specific features that are difficult to find and reproduce in GCC and PCC, respectively.

An important source of bCC is mollusc shells from aquaculture.[13,14] This is a farming sector of growing economic relevance and nowadays the production of mollusc shells by aquaculture is about 15 Mton per year.[15] The majority of these shells are not collected and become waste which represents a major economic and environmental issue.[15−18] Their valorization by sustainable and green processes is desirable and can be a good example of circular economy.[19]

Presently, mollusc shell powders are used as calcium integrator in poultry's feed, liming agents in agriculture, and inert filler in diverse composite materials.[13,16,20−22] When used as fillers, the bCC powders act as inert and do not provide any additional performance advantage to the material. Two examples are their application in polymers and concretes.

$CaCO_3$ is the most widely used inorganic filler in polymers.[23] GCCs are low in price and used primarily to reduce formula costs. By contrast, PCCs are higher in price and used to modify various properties of polymer composites.[2] Oyster shell powder imparted to ethylene-vinyl acetate/low-density polyethylene resulted in a material with a remarkably enhanced thermal stability and antimicrobial activity against Gram-positive and Gram-negative bacteria.[24] Mussel shell $CaCO_3$ was used as filler for a compostable matrix made of polylactic acid and poly(butylene adipate-*co*-terephthalate). In this case, thermal, mechanical, morphological, and physical investigations of these biocomposites showed that their performances were comparable with those produced with GCC.[25]

Eo and Yi prepared concrete with different oyster shell powder contents (10, 20, and 30 wt %) and found that the mechanical properties of concrete replaced by 10 wt % oyster shell powder were basically the same as that of ordinary concrete.[26] However, the use of oyster shell powder as fine aggregates had a negative impact on the durability of concrete.[27] It was reported that, when compared with ordinary concrete, the one enriched with oyster shell powder showed a higher water absorption.[28]

Hydrophobic modification of the surface of $CaCO_3$ is an effective method to improve its applications as filler in particular in the case of mollusc shell powder.[29] This surface treatment facilitates the dispersion in hydrophobic polymeric matrices, for example, preventing loss of mechanical performances, such as impact resistance. In addition, moisture pick-up by $CaCO_3$ may pose additional problems during handling and processing.[30] In concretes, it prevents water from penetrating concrete increasing corrosion resistance.[31]

Among a variety of $CaCO_3$ surface coaters such as silanes, phosphates, and titanates, the most widely used are fatty acids.[32] In particular, a blend of stearic acid and palmitic acid (stearin) and pure stearic acid are most commonly used for industrial applications and laboratory research, respectively. The process of stearic acid/stearate adsorption on the calcite surface can occur in "dry" conditions or by using "wet" methods.[33] Generally, the industrial coating is done in water because of the low cost and the simplicity of the process.[34,35] It has been suggested that in water suspension, in the presence of significant amounts of dissolved ions, the adsorption and subsequent rearrangement of fatty acid micelles is probably the controlling mechanism of coating rather than chemical surface adsorption.[34−36]

Here, we suppose that the stearate adsorption mechanism on bCC powders should be similar to that of GCC and PCC. This is because the process is mainly controlled by the presence of micelles of calcium stearate in aqueous dispersions.[34−36] However, we also suppose that the polymorphism, the crystalline texture, and the presence of the intracrystalline organic matrix, which are a unique signature of bCC and affect the structure and release of Ca ions,[37,38] may influence the adsorption capability of stearate. To test this hypothesis, we use bCC powders from waste seashells from aquaculture, namely oyster shells, scallop shells, and clam shells and compared the results with those obtained using GCC powder. Finally, the selected stearate-coated bCC sample was tested as a filler in an ethylene vinyl acetate compound used for the industrial preparation of shoe soles.

MATERIALS AND METHODS

Reagents and solvents were purchased from Sigma-Aldrich and utilized without any further purification. For each experiment, daily fresh solutions were prepared. Mollusc shells of *Crassostrea gigas* (oyster), *Pecten jacobaeus* (scallops), and *Chamelea gallina* (clams) were purchased from F.lli Terzi (Palosco, BG, Italy). Commercial GCC and stearate-coated (about 1.5 wt %) GCC were kindly provided by Finproject S.p.A.

Preparation of bCC Powders. Mollusc shells were first cleaned with tap water to eliminate mineral debris. Then, they were treated with a 5 vol % sodium hypochlorite solution for 24 h to remove the organic residues from the surface, washed with deionized water, and air-dried. The dry shells were finally crushed by a hammer mill and sieved at 45 μm by analytical sieving to remove the particles with a higher size. The bleached materials were obtained by milling each powder (15 g) with 15 vol % sodium hypochlorite solution (100 mL) for 72 h using a tube roller and ZrO_2 spheres (175 g). The suspension was then filtered under vacuum, and the powder was washed with deionized water, dried in an oven at 40 °C, and sieved at 45 μm.

Preparation of the Sodium Stearate Solution. Sodium stearate was first dissolved by adding it to water at 60 °C with a concentration of 40 or 400 mM. The mixture was stirred for about 30 min until a homogeneous dispersion was obtained.

$CaCO_3$ Coating with Stearate. The coating was carried out by adding 2.0 g of the $CaCO_3$ particles, biogenic or geogenic, to the sodium stearate solution (50 mL) at 60 °C. The suspension was stirred for 2 h. The coated $CaCO_3$ was then separated by vacuum filtration, thoroughly washed with water at 60 °C, and dried in an oven at 105 °C overnight.[34]

https://doi.org/10.1021/acsomega.3c06186
ACS Omega 2024, 9, 11232−11242

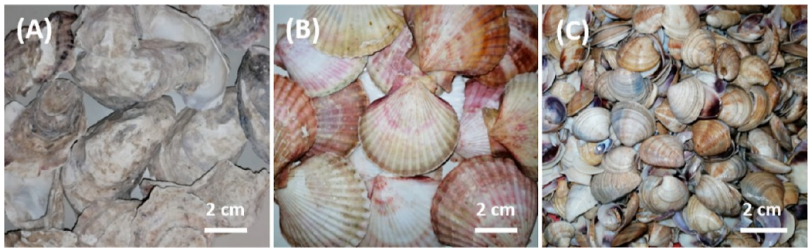

Figure 1. Camera images of pristine shells from the oyster *C. gigas* (A), the scallop *P. jacobaeus* (B), and the clam *C. gallina* (C).

Physical Characterization of the $CaCO_3$ Materials. X-ray diffraction patterns of the samples were collected using a PanAnalytical X'Pert Pro diffractometer equipped with a multiarray X'Celerator detector using Cu Kα radiation generated at 40 kV and 40 mA (λ = 1.54056 Å). The diffraction patterns were collected in the 2θ range between 20 and 60° for the starting materials and 1.5 and 12° for the coated ones with a step size ($\Delta 2\theta$) of 0.05° and a counting time of 60 s. The analysis of the diffraction pattern to obtain the polymorphic composition and crystallite dimensions was performed using Profex software.[39] FTIR spectra were collected by using a Thermo Scientific Nicolet iS10 FTIR spectrometer. Disk samples for FTIR analysis were prepared by mixing a small amount (2 mg) of sample with 98 mg of dry KBr and applying a pressure of 45 tsi (620.5 MPa) to the mixture using a press. The spectra were recorded with 4 cm^{-1} resolution and 64 scans. Scanning electron microscopy (SEM) measurements of the samples were acquired on a Carl Zeiss Leo 1530 Gemini field emission scanning electron microscope. The microscope was used with an accelerating voltage of 5 kV. The samples were glued on carbon tape, dried under vacuum in a desiccator, and 10 nm gold-coated before their observation. The size distribution measurements were performed with a Mastersizer 2000 (Malvern Panalytical Ltd.) laser diffraction particle size analyzer by dispersing bCC or GCC particles in isopropanol and measuring the distribution in isopropanol. Average value was calculated for five measurements. The specific surface area of the samples was measured by the multiple BET method using a Gemini VII 2390 Series surface area analyzer (Micromeritics Instrument Corp.) with a nitrogen flow. Thermogravimetric analysis (TGA) was carried out under nitrogen flow at a heating rate of 10 °C min^{-1} by a TA SDT Q600 V 8.0 instrument. The system was pre-equilibrated at 30 °C; then, a ramp from 30 to 900 °C was performed. For the measurement, 10 mg of each sample in an alumina crucible were used, and the temperature ranges considered to estimate the organic material and stearate content were different depending on the nature of the samples and were chosen based on the derivative thermogravimetric profiles (DTG). Differential scanning calorimetry (DSC) measurements were carried out under nitrogen flow at a heating rate of 10 °C min^{-1} from 0 to 200 °C with a TA Q100 instrument. The analysis was performed using 5 mg of each sample in a hermetic aluminum crucible to clarify the presence of hydrated calcium stearate. The contact angle with sessile water drops (volume of 10 μL) was measured using an optical system (Drop Shape Analyzer DSA30S, Krüss GmbH). Average values were calculated for five measurements on different points on each surface. The sample was compressed into a pellet before the measurement. Quantitative color measurements were acquired by an Eoptis CLM-194 colorimeter using a D65 light source and $BaSO_4$ as reference. The results were reported in the CIE $L^*a^*b^*$ system, where L^* represents brightness while a^* and b^* represent color parameters (a^* on the red-green scale and b^* on the yellow-blue scale).

$CaCO_3$ Elemental Composition. The sample was set in a Teflon holder with 0.5 mL of H_2O_2 (30 vol %, Carlo Erba) and 6 mL of HNO_3 (65 vol %, Honeywell). The holder was set in a microwave oven (Milestone) operating as follows: 2 min at 250 W, 2 min at 400 W, 1 min at 0 W, and 3 min at 750 W. The digested sample was quantitatively collected, diluted to 10 mL with water, and filtered on paper. All the liquid samples obtained were measured 3 times, 12 s each, with 60 s of prerunning, using a Spectro Arcos-Ametek ICP-OES analyzer. The calibration curve was made by using certified standards in water.

Synthesis of the Coated bCC/Ethylene Vinyl Acetate Compounds. The stearate-coated bCC/ethylene vinyl acetate compounds were prepared according to an industrial procedure. Briefly, polymers and raw materials, in the right mass ratio, were cold introduced into a closed mixer (Comerio Ercole S.p.A.). Through friction, the mixture reached the temperature of 90 °C and then was discharged into the hopper of a granulation extruder (Filmex SAS). Successively, the granules were introduced into the hopper of an injection press (Main Group), plasticized at 95 °C, and injected into the mold at about 200 °C, where the expansion and cross-linking reactions took place for a curing time of about 7 min. The specimens were cooled in a temperature-controlled environment at 23 °C and stored at the same temperature.

Mechanical and Esthetic Characterization of Polymeric Compounds. The mechanical and esthetic characterization of the polymeric compounds were performed after a preliminary specimen preparation in which a splitting machine (Camoga C420) was used to remove the external skins and a pneumatic cutter (NOSELAB ATS 10019000) was used for the preparation of specimens having the shape requested by the ISO regulation (Figure S1). For the measurement of the tensile strength and elongation at break, a Zwick/Roell Z010 dynamometer with a 10 kN load cell and Long Stroke extensometer with a 800 mm extension was used. The test was conducted according to the ASTM D 412 technical standard with a clamp removal speed of 200 mm min^{-1}. The esthetic features were evaluated by images obtained using an optical microscope under reflection conditions.

RESULTS AND DISCUSSION

In this work, we have employed seashells from species that (i) have a strong relevance in aquaculture,[13] (ii) are made of a single $CaCO_3$ polymorph, and (iii) have diverse crystalline textures.[15,38] The bCC used in this study are the low Mg-calcite from the oyster *C. gigas*, the medium Mg-calcite from

https://doi.org/10.1021/acsomega.3c06186
ACS Omega 2024, 9, 11232−11242

the scallop *P. jacobaeus*, and the aragonite clam *C. gallina* (Figure 1).

In analyzing their capability to be coated with stearate, the seashell powders were homogenized in grain size, performing ball milling and sieving at 45 μm. The same process was done for GCC as comparison. In addition, to evaluate the effects of the surface-exposed organic matrix, an aliquot of the bCC powder was bleached. The characteristics of the obtained powders are reported in Tables 1 and 2. The X-ray powder diffraction patterns (Figures S2 and S3) showed that in the powder from clam shells, upon the dry grinding process, a phase transition of about 10 wt % from aragonite to calcite occurred. This is in agreement with some literature data that reported that this phase transition is associated with the temperature increase produced by frictional heating of grinding[40,41] due to the highest thermodynamic stability of calcite[32] but disagrees with other research studies reporting the opposite.[42,43] The bleaching treatment in wet conditions favored this phase transition, and the content of calcite increased to about 19 wt %. A similar behavior was reported for abalone shells.[44] Interestingly, the content of intraskeletal organic material did not change in a relevant way after the bleaching process. This is due to the fact that the majority of the organic material is intracrystalline, and only the organic macromolecules on the grain surface are oxidized and removed by the bleaching process.[19] The surface area of the samples did not increase in a relevant way after the bleaching process, despite the decrease of the particle size, in both the biogenic and geogenic $CaCO_3$ samples. The latter observation suggests that the reduction in grain size is more related to the grinding associated with the bleaching process than the removal of organic macromolecules.

We excluded a process of dissolution and reprecipitation for GCC since the crystallite sizes ($d_{[104]}$), which were determined by the analyses of the powder X-ray diffraction profile, did not change relevantly. On the contrary, the crystalline domains of mollusc shell powder increased after the bleaching process. This could be due to a recrystallization process of the external layer of the crystallites that has been shown to be formed by amorphous calcium carbonate.[45,46]

The results of the elemental analyses are reported in Table 2 and agree with the expected elemental composition.[47] The concentration of calcium is around 40 wt %, and the content of magnesium is higher in scallop shells than in oyster shells, while strontium is present in a higher amount in the aragonite shell of the clam. The content of the other elements is quite low. After the bleaching process, only the concentration of the minor elements changed, probably due to the dissolution of some soluble salts present in traces in the pristine shells.

The morphological appearance of the obtained powder particles is shown in Figures 2 and S4. The geogenic calcite did not change the grain morphology upon the bleaching process, even if the particle size was reduced, in agreement with the grain size distribution (Figure 2A,B). Differently, the mollusc shell powders showed a change in the morphology of the particles because of the bleaching process (Figure 2C−H). This effect appears species-specific, being different in the texture, the polymorphism, and the composition among species. The oyster *C. gigas* shells are made of low Mg-calcite with an isomorphic substitution of magnesium to calcium of about 5 mol %.[48] Both valves of the adult oyster shell are predominantly composed of foliated calcite,[49] which is bound on the outermost surface by prismatic calcite and is interrupted by lenses of chalky calcite.[50] The image clearly shows that the (001) surface of the laths making the foliated calcite smooth before bleaching and becomes rough and highly porous (Figure 2C,D). This provokes a slight increase of the specific surface area, which mainly also contributes to the reduction of the grain size. The shell of the scallop *P. jacobaeus* is composed of calcite foliated layers,[49] except for a thin aragonitic prismatic pallial myostracum.[51] The content of Mg in the calcite

Table 1. Percentage $CaCO_3$ Polymorph, Organic Matrix Content, Particle Size D_{90}, Surface Area, and Crystallite Size of Calcite of GCC (A), Oyster Shell (B), Scallop Shell (C), and Clam Shell Powder (D) after 45 μm sieving[a]

sample	calcite (wt %)[b]	organic material content (wt %)[c]	D_{90} (μm)	surface area ($m^2\ g^{-1}$)	$d_{(104)}$[d] (nm)
A	99.0	0.2	19.39	2.9	79.7
B	100	1.3	32.55	3.9	103.9
C	100	0.8	29.01	4.6	84.1
D	9.5	0.6	24.41	4.0	66.5
A-b	99.0	0.2	4.34	4.0	69.4
B-b	100	1.3	6.88	5.9	209.0
C-b	100	0.7	4.60	5.2	134.6
D-b	19.8	0.5	7.72	3.5	93.4

[a]D_{90} indicates that up to 90 % of the total particles has a grain size smaller than the reported value. that the samples were subject to a bleaching/grinding process. [b]The complement to 100% is represented by quartz for sample A and aragonite for sample D. [c]The temperature range considered to estimate the organic material content was between 300 and 550 °C. [d]Crystallite size of calcite along the [104] direction.

Table 2. Elemental Composition of the Most Relevant Elements in Geogenic $CaCO_3$ (A), Oyster Shell (B), Scallop Shell (C), and Clam Shell Powder (D) after 45 μm Sieving[a]

<!—Col Count:7-->sample	Ca ($mg\ g^{-1}$)	Fe ($mg\ g^{-1}$)	K ($mg\ g^{-1}$)	Mg ($mg\ g^{-1}$)	Na ($mg\ g^{-1}$)	Sr ($mg\ g^{-1}$)
A	385	0.56	5.6	7.28	23.52	ND[b]
B	392	ND	0.56	1.68	3.36	0.56
C	379	ND	ND	2.8	2.8	1.12
D	373	ND	ND	ND	3.36	1.68
A-b	357	0.56	0.56	6.16	1.68	ND
B-b	382	ND	1.12	1.68	3.92	0.56
C-b	395	ND	1.12	2.24	2.8	1.12
D-b	378	ND	ND	ND	2.8	1.68

[a]The suffix -b indicates the samples that were subject to a bleaching/grinding process. [b]The concentration was below the instrumental detection limit.

https://doi.org/10.1021/acsomega.3c06186
ACS Omega 2024, 9, 11232−11242

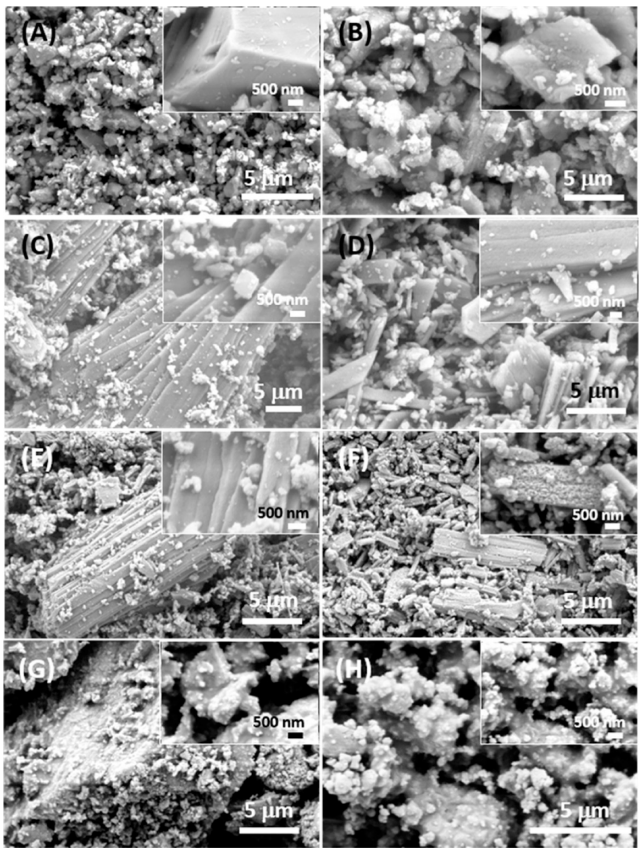

Figure 2. SEM images of unbleached (A,C,E,G) and bleached (B,D,F,H) powders from geogenic $CaCO_3$ (A,B), oyster shells (C,D), scallop shells (E,F), and clam shells (G,H). The insets report high-magnification images. These images are representative of the entire population of particles.

structure is of about 7 mol %.[48] As observed for the shell of *C. gigas,* the bleaching induced an increase of the surface roughness and porosity of the laths (Figure 2E,F), which is associated with an increase of the surface area. The aragonite shell of the clam *C. gallina* presents in the internal layer a granular texture in which the grains do not show any apparent microstructure and a thinner external prismatic layer. These structural motifs do not change their morphology in a relevant way after the bleaching process (Figure 2G,H), except for a reduction of the grain size, which is not associated with a relevant change of the surface area.

The samples were also evaluated in their color, which is an important parameter for industrial applications. White fillers are in great demand by the industry because they allow a better control of the coloring of the material given by pigments and dyes.[52] The data (Table S1) show that the brightness (L^*) of bleached samples is higher than that of the untreated ones. This value slightly increases for geogenic calcite (0.1%), while for oysters, scallops, and clams the increase was 2.4, 1.9, and 4.8%, respectively. In addition, the color distance from the white reference (dE^*ab^*) decreased moving from the unbleached to the bleached samples, it was 0.2% for the geogenic calcite, while for oysters, scallops, and clams it was 47, 14, and 93%, respectively. These improvements, which were higher for clams than for oysters and scallops, could be due to a lower efficiency of the bleaching process or a higher content of colored pigment present in clam shells.

The coating of the $CaCO_3$ particles was performed using 40 and 400 mM sodium stearate aqueous dispersions. These concentrations are both above the critical micellar concentration of stearate, which according to the literature is from 0.45 mM (at 20 °C) to 0.7 mM (at 60 °C).[53] In a similar reference experiment, Shi et al. (2010)[34] used a 400 mM sodium stearate aqueous dispersion with precipitated $CaCO_3$ crystals having a surface area of about 65 g m^{-2}. This value is about 10 times higher than that of the $CaCO_3$ powders used (Table 1). Therefore, we used 40 mM, and also 400 mM for comparison, sodium stearate aqueous dispersions.

The adsorbed amount of stearate was determined by the weight loss in TGA experiment (Table 3, Figures S5 and S6) in the range between about 250 and 500 °C. When 40 mM sodium stearate aqueous dispersion was used, the particles were able to adsorb slightly different amounts of stearate according to their source (Table 3), on the other hand, these differences were more marked when 400 mM stearate dispersion was used (Table 4). The biogenic calcite substrates, oyster, and scallop ground shells, adsorbed more stearate than the biogenic aragonite from clam shells and geogenic calcite.

Table 3. Thermal and Surface Analyses of Geogenic $CaCO_3$ (A), Oyster Shell (B), Scallop Shell (C), and Clam Shell Powder (D) Coated Using 40 mM Sodium Stearate Aqueous Dispersion[a]

sample	OM + St content (wt %)	adsorption capacity (mg m^{-2})	contact angle (deg)	crystalline-to-smectic (°C)	ΔH (J g^{-1})
A	4.5	15.5	139.4	125.5	2.9
B	4.7	9.0	137.7	126.1	3.0
C	4.7	9.1	133.4	125.4	2.3
D	4.4	9.9	147.5	126.2	2.5
A-b	4.7	12.3	150.1	125.4	2.5
B-b	5.2	6.9	135.0	125.2	2.6
C-b	5.4	9.5	146.3	126.1	2.1
D-b	4.4	11.6	159.0	125.5	2.7

[a]The temperature range considered to estimate the organic matrix (OM) and stearate (St) contents was selected according to the derivate profile of the thermogravimetric curve. The suffix -b indicates the samples that were subject to a bleaching/grinding process.

Table 4. Thermal and Surface Analyses of Geogenic $CaCO_3$ (A), Oyster Shell (B), Scallop Shell (C), and Clam Shell Powder (D) Coated Using 400 mM Sodium Stearate Aqueous Dispersion[a]

sample	OM + St content (wt %)	adsorption capacity (g m^{-2})	contact angle (deg)	crystalline-to-smectic (°C)	ΔH (J g^{-1})
A	10.2	27.2	135.4	126.4	10.1
B	23.1	60.9	136.4	126.4	18.6
C	13.1	20.2	137.3	125.6	18.9
D	11.7	20.9	139.0	126.1	8.6
A-b	13.2	25.3	149.0	126.4	9.2
B-b	26.9	45.1	92.2	126.2	15.4
C-b	14.0	18.6	146.3	126.3	10.2
D-b	14.5	35.3	128.8	125.9	10.3

[a]The temperature range considered to estimate the organic matrix (OM) and stearate (St) content was selected according to the derivate profile of the thermogravimetric curve. The suffix -b indicates the samples that were subject to a bleaching/grinding process.

https://doi.org/10.1021/acsomega.3c06186
ACS Omega 2024, 9, 11232−11242

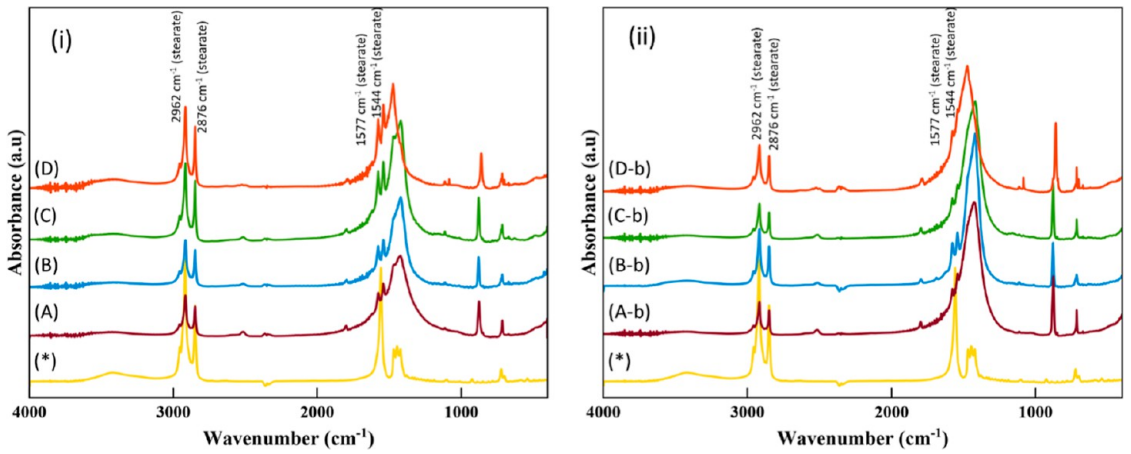

Figure 3. FTIR spectra of unbleached and bleached powders of (A) geogenic $CaCO_3$, (B) oyster shells, (C) scallop shells, and (D) clam shells coated using 400 mM stearate dispersion. (i) Unbleached $CaCO_3$ samples. (ii) Bleached $CaCO_3$ samples. (*) Sodium stearate spectrum.

Moreover, in all of the samples, the bleached substrates adsorbed a higher amount of stearate than the untreated ones. This effect, which can be related to the increase of the specific surface area after bleaching, was more marked for the biogenic calcite particles than for the biogenic aragonite.

The stearate was adsorbed on the $CaCO_3$ particles in the form of a Ca salt. These results can be explained by considering that less soluble calcium stearate forms by the exchange reaction between Na stearate and Ca ions in the water suspension.[54] As a consequence, Ca ions dissolve from uncoated areas of the surface of $CaCO_3$ particles to restore equilibrium until only calcium stearate is present. The surface area covered by one molecule of the stearate at the equilibrium is one important parameter that depends on the crystal faces exposed by the $CaCO_3$ particles.[36] Kralj et al. reported the cross-sectional area of one stearate molecule of 0.21 nm^2 on rhombohedral {104} calcite planes and 0.31 nm^2 for scalenohedral {211} planes in nonstoichiometric calcites.[55] Also, the arrangement of the stearate molecules influences the cross-sectional area.[56] Assuming a cross-sectional area of stearate of 0.2 nm^2, which corresponds to the surface area for one stearate molecule in a perpendicular orientation,[57] for the mean surface areas of $CaCO_3$ particles used (5 m^2 g^{-1}) the theoretical full monolayer coverage would be about 1.2 wt % for stearate coating. At both concentrations investigated in this study, the amount of stearate adsorbed is beyond the theoretical monolayer coverage as shown in Tables 3 and 4. This indicates that the stearate on the $CaCO_3$ particle surface exists in a multilayer form, with the number of layers increasing as the amount of stearate increases.

The adsorbed Ca stearate on the $CaCO_3$ particle surface can be expected to have complex calorimetric properties since the process conditions used during water coating can favor the formation of its hydrate form, calcium stearate monohydrate.[58] The DSC profiles (Figures S7 and S8) show, as the temperature increases, first a dehydration peak (115 °C) and then a peak corresponding to the transitions from the crystalline-to-smectic phase (130 °C), which agrees with what is reported in the literature for this material.[59] The relationship between the dehydration enthalpy and the crystalline-to-smectic transition enthalpy for the Ca stearate layer adsorbed on the $CaCO_3$ particles surface versus the adsorbed amount of stearate, determined by DSC measurement, is presented in Figure S9. Both enthalpies increase linearly as the adsorbed amount of stearate increases when 400 mM stearate dispersion was used. Because the crystalline-to-smectic peak and dehydration peaks in the DSC measurements belong to only the physically adsorbed part of Ca stearate, it means that the physically adsorbed part increases in a proportional way to the total organic amount of surfactant and that the chemisorbed part remains at a constant value for each substrate. This observation is also confirmed by the data regarding the contact angle (Tables 3 and 4) that show how this value is almost constant among all samples, with the exception of the sample of oyster powder treated with 400 mM sodium stearate aqueous dispersion. The variation among samples could be related to the surface morphology, which is known to affect the contact angle.[60,61] All the samples showed a similar temperature of the crystalline-to-smectic transition, while the enthalpy associated with this process was higher for the sample prepared in the presence of 400 mM sodium stearate aqueous dispersion. This observation could be related to the size of the crystalline domains of the physically adsorbed part of Ca stearate layers,[62] but this has not been investigated in the present study.

Important information comes from the evaluation of the adsorption capacity (Tables 3 and 4), that here it is defined as the mass of stearate for the surface unit of the $CaCO_3$ particles. The data clearly show that when 40 mM stearate dispersion was used the GCC and the oyster shell powder adsorbed the highest amount of stearate for the surface unit, but when 400 mM stearate dispersion was used the oyster shell powder showed an absorption capacity higher than GCC.

The rationalization of this observation needs to recall the specific features of the bCC. Among them, the presence of the intraskeletal organic matrix, which is the highest in oyster shell powder among the samples analyzed. Its presence destabilizes the calcium carbonate structure and thus increases its solubility.[63,64] Thus, according to the proposed mechanism that implies the formation of calcium stearate, a higher amount of this salt is formed during the interaction between the stearate micelles and the powder.

The structure of the adsorbed stearate was further investigated by SEM, FTIR, and X-ray powder diffraction. In Figure 3, the FTIR spectra of $CaCO_3$ particles coated by using 400 mM dispersion of stearate are shown. The two bands at about 2919 and 2852 cm^{-1} are due to the antisymmetric and symmetric methyl stretching vibration modes (ν_{aCH_3} and

https://doi.org/10.1021/acsomega.3c06186
ACS Omega 2024, 9, 11232−11242

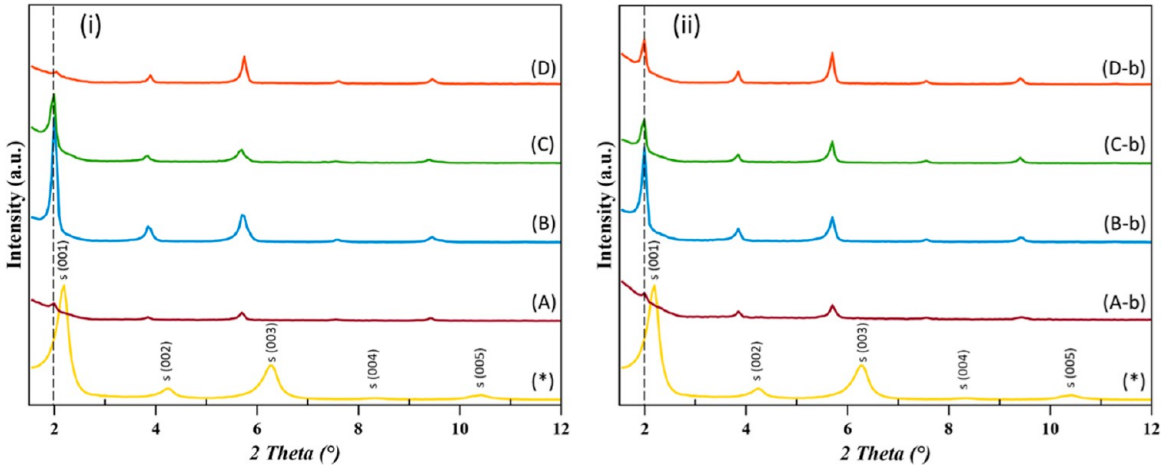

Figure 4. X-ray powder diffraction patterns of powders of (A) geogenic $CaCO_3$, (B) oyster shells, (C) scallop shells, and (D) clam shells coated using 400 mM stearate dispersion. (i) Unbleached $CaCO_3$ samples. (ii) Bleached $CaCO_3$ samples. (*) Sodium stearate diffraction pattern.

ν_{sCH_3}), respectively. The absorption bands at 1577 and 1544 cm^{-1} are due to the antisymmetric ν_{aCOO^-} stretching vibration of carboxylate groups in unidendate and bidendate coordination with Ca ions, respectively.[65] No other bands associated with carboxylate groups were present, thus only calcium stearate was formed.[35] Other absorption bands are due to vibrational modes associated with calcite and aragonite or due to the alkyl chains of the stearate. No band shift was observed among samples, and only the relative intensities of the bands changed according to the composition of stearate/calcium carbonate materials. When 40 mM stearate dispersion was used, the low relative amount of adsorbed stearate (Table 3) did not allow its detection, and the FTIR spectra showed only the typical adsorption bands of calcite and aragonite (Figure S10).

The examination of powder X-ray diffraction patterns of the materials provided information on the crystal form of calcium carbonate (Mg-calcite or aragonite) and also on the structure of its stearate coating.

The diffraction peaks at small Bragg angles ($2\theta < 12°$) from the coated particles using the 40 mM stearate dispersion (Figure S11) did not show diffraction peaks for the unbleached samples, which contained the lowest percentage of stearate (Table 3). The only exception was observed when oyster powder was used. In this case, a weak diffraction peak was detected at 1.98°. Using the same stearate dispersion, the associated diffraction peaks were detected in the bleached samples. These were at 2θ values of 1.98, 3.90, 5.72, 7.59, and 9.48° corresponding to the first five orders of the laminar structure of calcium stearate (46.5 Å) having extended chains oriented almost normal to the plane containing the ionic groups.[66] When 400 mM stearate dispersion was used, the low-angle diffraction peaks were more intense as expected having a higher concentration of stearate (Figure 4). This effect was more evident for the bleached samples (Table 4). Also, in this set of experiments, it can be noted that the oyster shell powder was the substrate with the most intense calcium stearate diffraction peaks.

The absence of diffraction peaks in the samples with the lower content of stearate could be due to the detection limit of the method but also because the chemisorbed stearate does not give diffraction peaks as previously reported.[34] Thus, where diffraction peaks are detected, the majority of calcium stearate is physisorbed on the surface of stearate-chemisorbed $CaCO_3$ particles.

The SEM images of the samples treated with 40 and 400 mM stearate dispersion are reported in Figures 5 and 6, respectively. The samples treated with 40 mM stearate

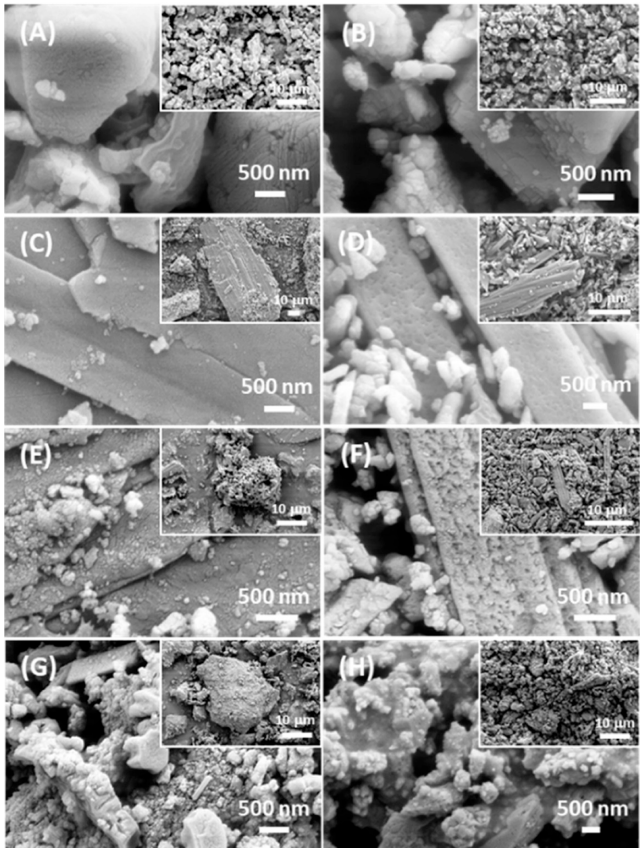

Figure 5. SEM images of $CaCO_3$ particles coated using 40 mM stearate dispersion. (A) Geogenic $CaCO_3$, (B) bleached geogenic $CaCO_3$, (C) oyster shell powder, (D) bleached oyster shell powder, (E) scallop shell powder, (F) bleached scallop shell powder, (G) clam shell powder, and (H) bleached clam shell powder. The insets report a low-magnification image for each sample. The images are representative of the entire population of particles.

https://doi.org/10.1021/acsomega.3c06186
ACS Omega 2024, 9, 11232−11242

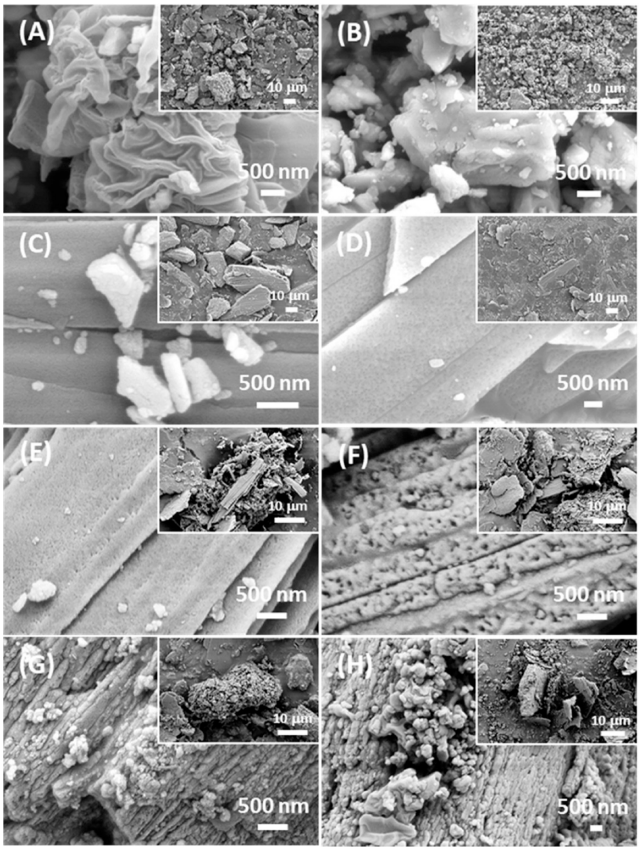

Figure 6. SEM images of $CaCO_3$ particles coated using 400 mM stearate dispersion. (A) Geogenic $CaCO_3$, (B) bleached geogenic $CaCO_3$, (C) oyster shell powder, (D) bleached oyster shell powder, (E) scallop shell powder, (F) bleached scallop shell powder, (G) clam shell powder, and (H) bleached clam shell powder. The insets report a low-magnification image of each sample. The images are representative of the entire population of particles.

dispersion (Figure 5) generally preserve all of the textural and morphological features of the samples before the coating process. This is expected since a low amount of stearate is adsorbed, no more than a few layers, on the unbleached samples. These layers do not change the overall morphology and do not induce a relevant aggregation of the particles. The higher amount of stearate adsorbed on the bleached samples does not change in a relevant way the morphology of the particles, even if the X-ray data indicate that the presence of crystalline layers is able to generate a diffraction pattern. The $CaCO_3$ particles treated with 400 mM stearate dispersion and containing a high percentage of stearate lose many of the surface characteristics of the uncoated samples (Figure 6). Moreover, the presence of deposits of layered structures, which may embed $CaCO_3$ particles, is observable.

According to the reported data in the aqueous coating using a hot dispersion of sodium stearate, a chemisorbed-monolayer first forms on which the precipitation of micelles generates additional physically adsorbed layers of calcium stearate. During the deposition/drying process, the aliphatic groups reorganize and orient outward of the surface, leading to a hydrophobic $CaCO_3$ surface and a low surface energy.[34,35] Moreover, the diverse textures and polymorphisms of the bCC favor the chemical−physical processes associated with the adsorption process, generating stacked multilayers,[67] being this effect particularly marked for the oyster shell powder.

Some of the prepared materials were finally tested as fillers in an ethylene vinyl acetate compound for the preparation of shoe soles. The $CaCO_3$ particles were used in a 10 wt % concentration as commonly done in the industrial process. We tested the oyster shell coated materials, since they were the substrates with the highest capability of stearate adsorption. The process was performed according to the industrial procedure, thus, giving room for future potential scale-up. In a separate set, the ethylene vinyl acetate matrices were loaded with the same mass percentage of 45 μm sieved commercial stearate-coated GCC as the control. The optical images in Figure 7 show that the foamability, the qualitative distribution of pores, of the shoe soles did not change when the commercial stearate-coated GCC was replaced with the bCC coated with different amounts of stearate. This is an important parameter that affects the overall esthetic feature of the compound[68] and thus its commercialization.

The data reported in Figure 8 show that the oyster powder coated with stearate improved the maximum elongation at break with respect to the control, and this effect was more marked when the sample with the lower percentage of adsorbed stearate was used. The improvement was about 55%. No relevant improvement on tensile strength, being about 10%, was observed. Both sets of data indicate that a too high amount of physiosorbed calcium stearate has a negative effect on the mechanical performances of the ethylene vinyl acetate/$CaCO_3$ composite material. The deleterious effect of the high amount of adsorbed stearate was also reported for an ethylene vinyl acetate composite containing stearate-coated $Mg(OH)_2$ crystals.[69]

CONCLUSIONS

This study has shown that bCC from waste seashells can be successfully coated by using an aqueous dispersion of sodium stearate. All of the experimental data indicate that the adsorption process is similar to that already reported for synthetic and geogenic calcite. Shortly, a first layer of

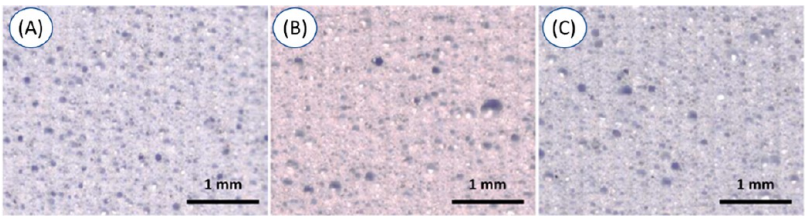

Figure 7. SEM images of the $CaCO_3$/ethylene vinyl acetate compound. (A) Compound obtained using commercial stearate-coated geogenic $CaCO_3$ particles. (B) Compound obtained using oyster shell particles coated with 40 mM stearate dispersion. (C) Compound obtained using oyster shell particles coated with 400 mM stearate dispersion.

https://doi.org/10.1021/acsomega.3c06186
ACS Omega 2024, 9, 11232−11242

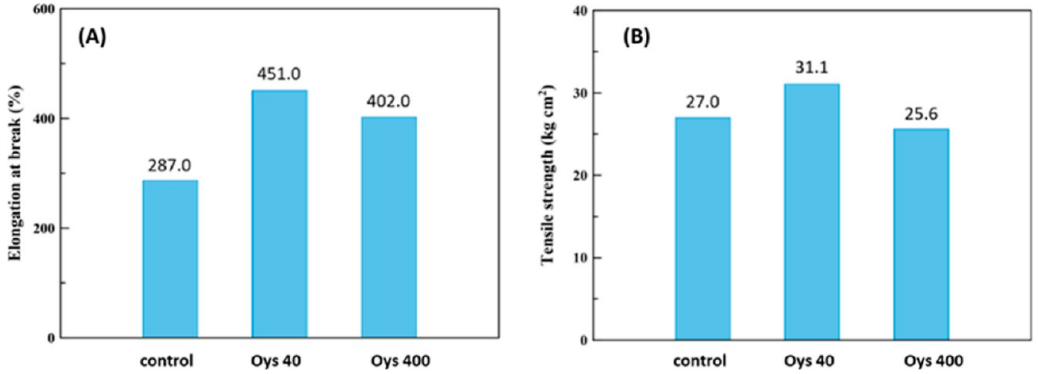

Figure 8. Mechanical characterization. (A) Elongation to break and (B) tensile strength of $CaCO_3$/ethylene vinyl acetate compounds. The control is the compound prepared using a commercial sample of stearate-oated geogenic $CaCO_3$. Oys_{40} and Oys_{400} indicate oyster shell powders coated using 40 and 400 mM stearate dispersion, respectively.

chemisorbed stearate is followed by the deposition of several layers of physiosorbed calcium stearate. However, the peculiar texture and composition of bCC affect the adsorption capacity of the substrate, being particularly efficient in the case of oyster shell powders. The coated oyster powder has been utilized as a filler in an ethylene vinyl acetate compound and improved the mechanical properties with respect to a control using commercial stearate-coated calcium carbonate. Finally, we can conclude that this work demonstrates that it is possible to recover calcium carbonate from seashells for application as fillers in replacement for geogenic calcium carbonate, thus improving the circularity and the sustainability of the industries as in the studied case of ethylene vinyl acetate compounds. It is also important to note that the approach to recycle, preserving the peculiar features of seashells, has a wide applicability to all biominerals, expanding the potential utilization of this methodology.

■ ASSOCIATED CONTENT

Supporting Information

The Supporting Information is available free of charge at https://pubs.acs.org/doi/10.1021/acsomega.3c06186.

SEM images, TGA profiles, DSC profiles, and XRD patterns (PDF)

■ AUTHOR INFORMATION

Corresponding Author

Giuseppe Falini − *Department of Chemistry "Giacomo Ciamician", University of Bologna, 40126 Bologna, Italy;* orcid.org/0000-0002-2367-3721; Email: giuseppe.falini@unibo.it

Authors

Maria Luisa Basile − *Department of Chemistry "Giacomo Ciamician", University of Bologna, 40126 Bologna, Italy*

Carla Triunfo − *Department of Chemistry "Giacomo Ciamician", University of Bologna, 40126 Bologna, Italy; Fano Marine Center, 61032 Fano, Italy*

Stefanie Gärtner − *Department of Chemistry, Physical Chemistry, University of Konstanz, D-78457 Konstanz, Germany*

Simona Fermani − *Department of Chemistry "Giacomo Ciamician", University of Bologna, 40126 Bologna, Italy; Interdepartmental Centre for Industrial Research Health Sciences & Technologies, University of Bologna, 40064 Bologna, Italy*

Davide Laurenzi − *Plant Ascoli Piceno, Finproject S.p.A., 3100 Ascoli Piceno, Italy*

Gabriele Maoloni − *Plant Ascoli Piceno, Finproject S.p.A., 3100 Ascoli Piceno, Italy*

Martina Mazzon − *DiSTA, Department of Science and Technology of Agriculture and Environment, University of Bologna, 40127 Bologna, Italy;* orcid.org/0000-0001-5136-0135

Claudio Marzadori − *DiSTA, Department of Science and Technology of Agriculture and Environment, University of Bologna, 40127 Bologna, Italy*

Alessio Adamiano − *Institute of Science, Technology and Sustainability for Ceramics, Consiglio Nazionale delle Ricerche, 48018 Faenza, Italy;* orcid.org/0000-0002-2077-0411

Michele Iafisco − *Institute of Science, Technology and Sustainability for Ceramics, Consiglio Nazionale delle Ricerche, 48018 Faenza, Italy;* orcid.org/0000-0002-7813-8347

Devis Montroni − *Department of Chemistry "Giacomo Ciamician", University of Bologna, 40126 Bologna, Italy*

Jaime Gómez Morales − *Laboratorio de Estudios Cristalográficos, Instituto Andaluz de Ciencias de la Tierra (CSIC-UGR), 18100 Armilla, Granada, Spain;* orcid.org/0000-0002-9395-7797

Helmut Cölfen − *Department of Chemistry, Physical Chemistry, University of Konstanz, D-78457 Konstanz, Germany;* orcid.org/0000-0002-1148-0308

Complete contact information is available at: https://pubs.acs.org/10.1021/acsomega.3c06186

Author Contributions

The manuscript was written through the contributions of all authors. All authors have given approval to the final version of the manuscript. M.L.B., C.T., and S.G. contributed equally.

Funding

Italian Minister of University and Research, MIUR ERA-NET Cofund on Blue Bioeconomy (BlueBio) project CASEAWA (grant agreement ERA-NET no. 817992).

Notes

The authors declare no competing financial interest.

■ ACKNOWLEDGMENTS

G.F., C.T., S.F., D.L., G.M., J.G.M., S.G., and H.C. thank the respective national funding agency members of the call BlueBio ERANET. J.G.M. acknowledges grant no. PCI2020-112108 (MCIN/AEI/10.13039/501100011033 and "NextGenerationEU/PRTR"). G.F. and S.F. thank the National Recovery and Resilience Plan (NRRP), Mission 4 Component 2 Investment 1.4—Call for tender no. 3138 of 16 December 2021, rectified by Decree no. 3175 of 18 December 2021 of Italian Ministry of University and Research funded by the European Union—NextGenerationEU, project code CN_00000033, Concession Decree no. 1034 of 17 June 2022 adopted by the Italian Ministry of University and Research, Project title "National Biodiversity Future Center—NBFC". G.F. and C.M. thank Dr. Andrea Simoni for the support in the ICP-OES measurements. We thank Dr. Franco Corticelli (IMM-CNR) for the help in the SEM observation.

■ REFERENCES

(1) Calcium carbonate market—growth, trends, and forecasts. https://www.mordorintelligence.com/industry-reports/calcium-carbonate-market, 2023.
(2) Jimoh, O. A.; Ariffin, K. S.; Hussin, H. B.; Temitope, A. E. Synthesis of Precipitated Calcium Carbonate: A Review. *Carbonates Evaporites* **2018**, *33*, 331−346.
(3) Chen, Z.; Nan, Z. Controlling the Polymorph and Morphology of CaCO3 Crystals Using Surfactant Mixtures. *J. Colloid Interface Sci.* **2011**, *358* (2), 416−422.
(4) Erdogan, N.; Eken, H. A. Precipitated Calcium Carbonate Production, Synthesis and Properties. *Physicochem. Probl. Miner. Process.* **2017**, *53*, 57−68.
(5) Agnihotri, R.; Mahuli, S. K.; Chauk, S. S.; Fan, L.-S. Influence of Surface Modifiers on the Structure of Precipitated Calcium Carbonate. *Ind. Eng. Chem. Res.* **1999**, *38* (6), 2283−2291.
(6) Watabe, N. Crystal Growth of Calcium Carbonate in the Invertebrates. *Prog. Cryst. Growth Charact.* **1981**, *4* (1−2), 99−147.
(7) Lowenstam, H. A.; Weiner, S. *On Biomineralization*; Oxford University Press on Demand, 1989.
(8) Gilbert, P. U. P. A.; Bergmann, K. D.; Boekelheide, N.; Tambutté, S.; Mass, T.; Marin, F.; Adkins, J. F.; Erez, J.; Gilbert, B.; Knutson, V.; et al. Biomineralization: Integrating Mechanism and Evolutionary History. *Sci. Adv.* **2022**, *8* (10), No. eabl9653.
(9) Marin, F.; Le Roy, N.; Marie, B. The Formation and Mineralization of Mollusk Shell. *Front. Biosci.* **2012**, *4*, 1099−1125.
(10) Knoll, A. H. Biomineralization and Evolutionary History. *Rev. Mineral. Geochem.* **2003**, *54* (1), 329−356.
(11) Berman, A.; Hanson, J.; Leiserowitz, L.; Koetzle, T. F.; Weiner, S.; Addadi, L. Biological Control of Crystal Texture: A Widespread Strategy for Adapting Crystal Properties to Function. *Science* **1993**, *259* (5096), 776−779.
(12) Honig, A.; Etter, R.; Pepperman, K.; Morello, S.; Hannigan, R. Site and Age Discrimination Using Trace Element Fingerprints in the Blue Mussel, Mytilus Edulis. *J. Exp. Mar. Biol. Ecol.* **2020**, *522*, 151249.
(13) Morris, J. P.; Backeljau, T.; Chapelle, G. Shells from Aquaculture: A Valuable Biomaterial, Not a Nuisance Waste Product. *Rev. Aquac.* **2019**, *11*, 42−57.
(14) Nekvapil, F.; Aluas, M.; Barbu-Tudoran, L.; Suciu, M.; Bortnic, R.-A.; Glamuzina, B.; Pinzaru, S. C. From Blue Bioeconomy toward Circular Economy through High-Sensitivity Analytical Research on Waste Blue Crab Shells. *ACS Sustain. Chem. Eng.* **2019**, *7* (19), 16820−16827.
(15) FAO. *The State of World Fisheries and Aquaculture*. Sustained Action, 2020.
(16) Hart, A. Mini-Review of Waste Shell-Derived Materials' Applications. *Waste Manage. Res.* **2020**, *38* (5), 514−527.
(17) Yan, N.; Chen, X. Don't Waste Seafood Waste: Turning Cast-off Shells into Nitrogen-Rich Chemicals Would Benefit Economies and the Environment. *Nature* **2015**, *524* (7564), 155−157.
(18) Topić Popović, N.; Lorencin, V.; Strunjak-Perović, I.; Čož-Rakovac, R. Shell Waste Management and Utilization: Mitigating Organic Pollution and Enhancing Sustainability. *Appl. Sci.* **2023**, *13* (1), 623.
(19) Magnabosco, G.; Giuri, D.; Di Bisceglie, A. P.; Scarpino, F.; Fermani, S.; Tomasini, C.; Falini, G. New Material Perspective for Waste Seashells by Covalent Functionalization. *ACS Sustain. Chem. Eng.* **2021**, *9* (18), 6203−6208.
(20) Summa, D.; Lanzoni, M.; Castaldelli, G.; Fano, E. A.; Tamburini, E. Trends and Opportunities of Bivalve Shells' Waste Valorization in a Prospect of Circular Blue Bioeconomy. *Resources* **2022**, *11* (5), 48.
(21) Khrunyk, Y.; Lach, S.; Petrenko, I.; Ehrlich, H. Progress in Modern Marine Biomaterials Research. *Mar. Drugs* **2020**, *18* (12), 589.
(22) Ruiz-Salmón, I.; Laso, J.; Margallo, M.; Villanueva-Rey, P.; Rodríguez, E.; Quinteiro, P.; Dias, A. C.; Almeida, C.; Nunes, M. L.; Marques, A.; et al. Life Cycle Assessment of Fish and Seafood Processed Products-a Review of Methodologies and New Challenges. *Sci. Total Environ.* **2021**, *761*, 144094.
(23) Owuamanam, S.; Cree, D. Progress of Bio-Calcium Carbonate Waste Eggshell and Seashell Fillers in Polymer Composites: A Review. *J. Compos. Sci.* **2020**, *4* (2), 70.
(24) Park, K.; Sadeghi, K.; Panda, P. K.; Seo, J.; Seo, J. Ethylene Vinyl Acetate/Low-Density Polyethylene/Oyster Shell Powder Composite Films: Preparation, Characterization, and Antimicrobial Properties for Biomedical Applications. *J. Taiwan Inst. Chem. Eng.* **2022**, *134*, 104301.
(25) Gigante, V.; Cinelli, P.; Righetti, M. C.; Sandroni, M.; Tognotti, L.; Seggiani, M.; Lazzeri, A. Evaluation of Mussel Shells Powder as Reinforcement for Pla-Based Biocomposites. *Int. J. Mol. Sci.* **2020**, *21* (15), 5364.
(26) Eo, S.-H.; Yi, S.-T. Effect of Oyster Shell as an Aggregate Replacement on the Characteristics of Concrete. *Mag. Concr. Res.* **2015**, *67* (15), 833−842.
(27) Mo, K. H.; Alengaram, U. J.; Jumaat, M. Z.; Lee, S. C.; Goh, W. I.; Yuen, C. W. Recycling of Seashell Waste in Concrete: A Review. *Constr. Build. Mater.* **2018**, *162*, 751−764.
(28) Song, Q.; Wang, Q.; Xu, S.; Mao, J.; Li, X.; Zhao, Y. Properties of Water-Repellent Concrete Mortar Containing Superhydrophobic Oyster Shell Powder. *Constr. Build. Mater.* **2022**, *337*, 127423.
(29) Rong, M. Z.; Zhang, M. Q.; Ruan, W. H. Surface Modification of Nanoscale Fillers for Improving Properties of Polymer Nanocomposites: A Review. *Mater. Sci. Technol.* **2006**, *22* (7), 787−796.
(30) Kato, T.; Sugawara, A.; Hosoda, N. Calcium Carbonate-Organic Hybrid Materials. *Adv. Mater.* **2002**, *14* (12), 869−877.
(31) Wei, J.; Wang, Z.; Sun, W.; Yang, R. Durability Performance and Corrosion Mechanism of New Basalt Fiber Concrete under Organic Water Environment. *Materials* **2023**, *16* (1), 452.
(32) Niu, Y.-Q.; Liu, J.-H.; Aymonier, C.; Fermani, S.; Kralj, D.; Falini, G.; Zhou, C.-H. Calcium Carbonate: Controlled Synthesis, Surface Functionalization, and Nanostructured Materials. *Chem. Soc. Rev.* **2022**, *51*, 7883−7943.
(33) Mihajlović, S. R.; Vučinić, D. R.; Sekulić, Ž. T.; Milićević, S. Z.; Kolonja, B. M. Mechanism of Stearic Acid Adsorption to Calcite. *Powder Technol.* **2013**, *245*, 208−216.
(34) Shi, X.; Rosa, R.; Lazzeri, A. On the Coating of Precipitated Calcium Carbonate with Stearic Acid in Aqueous Medium. *Langmuir* **2010**, *26* (11), 8474−8482.
(35) Shi, X.; Bertóti, I.; Pukánszky, B.; Rosa, R.; Lazzeri, A. Structure and Surface Coverage of Water-Based Stearate Coatings on Calcium Carbonate Nanoparticles. *J. Colloid Interface Sci.* **2011**, *362* (1), 67−73.
(36) Rothon, R.; Paynter, C. Calcium Carbonate Fillers. In *Fillers for Polymer Applications*; Rothon, R., Ed.; Springer International Publisher: Cham, Switzerland, 2017; pp 149−160.

https://doi.org/10.1021/acsomega.3c06186
ACS Omega 2024, 9, 11232−11242

(37) Addadi, L.; Weiner, S. Biomineralization: Mineral Formation by Organisms. *Phys. Scr.* **2014**, *89*, 098003.
(38) Marin, F.; Luquet, G. Unusually Acidic Proteins in Biomineralization. In *Handbook of Biomineralization: Biological Aspects and Structure Formation*; WILEY-VCH Verlag GmbH & Co. KGaA, 2007; pp 273−290.
(39) Doebelin, N.; Kleeberg, R. Profex: A Graphical User Interface for the Rietveld Refinement Program BGMN. *J. Appl. Crystallogr.* **2015**, *48* (5), 1573−1580.
(40) Gammage, R. B.; Glasson, D. R. The Effect of Grinding on the Polymorphs of Calcium Carbonate. *J. Colloid Interface Sci.* **1976**, *55* (2), 396−401.
(41) Momota, H.; Senna, M.; Takagi, M. Effects of Wet Vibro-Milling on the Polymorphic Conversion of Aragonite into Calcite. *J. Chem. Soc., Faraday Trans. 1* **1980**, *76*, 790−796.
(42) Burns, J. H.; Bredig, M. A. Transformation of Calcite to Aragonite by Grinding. *J. Chem. Phys.* **1956**, *25* (6), 1281.
(43) Li, T.; Sui, F.; Li, F.; Cai, Y.; Jin, Z. Effects of Dry Grinding on the Structure and Granularity of Calcite and Its Polymorphic Transformation into Aragonite. *Powder Technol.* **2014**, *254*, 338−343.
(44) Garcia, F.; Le Bolay, N.; Frances, C. Changes of Surface and Volume Properties of Calcite during a Batch Wet Grinding Process. *Chem. Eng. J.* **2002**, *85* (2−3), 177−187.
(45) Segovia-Campos, I.; Martignier, A.; Filella, M.; Jaquet, J.; Ariztegui, D. Micropearls and Other Intracellular Inclusions of Amorphous Calcium Carbonate: An Unsuspected Biomineralization Capacity Shared by Diverse Microorganisms. *Environ. Microbiol.* **2022**, *24* (2), 537−550.
(46) Politi, Y.; Arad, T.; Klein, E.; Weiner, S.; Addadi, L. Sea Urchin Spine Calcite Forms via a Transient Amorphous Calcium Carbonate Phase. *Science* **2004**, *306* (5699), 1161−1164.
(47) Turekian, K. K.; Armstrong, R. L. Magnesium, Strontium and Barium Concentrations and Calcite-Aragonite Ratios of Some Recent Molluscan Shells. *J. Mar. Res.* **1960**, *18*, 133−151.
(48) Long, X.; Ma, Y.; Qi, L. Biogenic and Synthetic High Magnesium Calcite - A Review. *J. Struct. Biol.* **2014**, *185* (1), 1−14.
(49) Boggild, O. B. *The Shell Structure of the Mollusks*; Det Kongelige Danske Videnskabernes Selskabs Skrifter. Naturvidenskabelig og Mathematisk Afdeling, Raekke 9; Andr. Fred Host & Son, 1930; Vol. *2*, pp 231−326.
(50) Checa, A. G.; Harper, E. M.; González-Segura, A. Structure and Crystallography of Foliated and Chalk Shell Microstructures of the Oyster Magallana: The Same Materials Grown under Different Conditions. *Sci. Rep.* **2018**, *8* (1), 7507.
(51) Grefsrud, E. S.; Dauphin, Y.; Cuif, J.-P.; Denis, A.; Strand, Ø. Modifications in Microstructure of Cultured and Wild Scallop Shells (Pecten Maximus). *J. Shellfish Res.* **2008**, *27* (4), 633−641.
(52) Berns, R. S. *Billmeyer and Saltzman's Principles of Color Technology*; John Wiley & Sons: Hoboken, NJ, USA, 2019.
(53) de Mul, M. N. G.; Davis, H. T.; Evans, D. F.; Bhave, A. V.; Wagner, J. R. Solution Phase Behavior and Solid Phase Structure of Long-Chain Sodium Soap Mixtures. *Langmuir* **2000**, *16* (22), 8276−8284.
(54) Fenter, P.; Sturchio, N. C. Structure and Growth of Stearate Monolayers on Calcite: First Results of an in Situ X-Ray Reflectivity Study. *Geochim. Cosmochim. Acta* **1999**, *63* (19−20), 3145−3152.
(55) Ukrainczyk, M.; Kontrec, J.; Kralj, D. Precipitation of Different Calcite Crystal Morphologies in the Presence of Sodium Stearate. *J. Colloid Interface Sci.* **2009**, *329* (1), 89−96.
(56) Wright, E. H. M.; Pratt, N. C. Solid/Solution Interface Equilibria for Aromatic Molecules Adsorbed from Non-Aromatic Media. Part 2.—Aromatic Carboxylic Acids. *J. Chem. Soc., Faraday Trans. 1* **1974**, *70*, 1461−1471.
(57) Fekete, E.; Pukánszky, B.; Tóth, A.; Bertóti, I. Surface Modification and Characterization of Particulate Mineral Fillers. *J. Colloid Interface Sci.* **1990**, *135* (1), 200−208.
(58) Garnier, P.; Gregoire, P.; Montmitonnet, P.; Delamare, F. Polymorphism of Crystalline Phases of Calcium Stearate. *J. Mater. Sci.* **1988**, *23*, 3225−3231.
(59) Höhne, G. W. H.; Hemminger, W.; Flammersheim, H.-J. *Differential Scanning Calorimetry*; Springer, 2003; Vol. *2*.
(60) Pechook, S.; Pokroy, B. Bioinspired Hierarchical Super-hydrophobic Structures Formed by N-Paraffin Waxes of Varying Chain Lengths. *Soft Matter* **2013**, *9* (24), 5710−5715.
(61) Pechook, S.; Kornblum, N.; Pokroy, B. Bio-Inspired Super-oleophobic Fluorinated Wax Crystalline Surfaces. *Adv. Funct. Mater.* **2013**, *23*, 4572−4576.
(62) Frey, M. H.; Payne, D. A. Grain-Size Effect on Structure and Phase Transformations for Barium Titanate. *Phys. Rev. B* **1996**, *54* (5), 3158−3168.
(63) Morse, J. W.; Arvidson, R. S.; Lüttge, A. Calcium Carbonate Formation and Dissolution. *Chem. Rev.* **2007**, *107* (2), 342−381.
(64) Busenberg, E.; Niel Plummer, L. Thermodynamics of Magnesian Calcite Solid-Solutions at 25 C and 1 Atm Total Pressure. *Geochim. Cosmochim. Acta* **1989**, *53* (6), 1189−1208.
(65) Gonen, M.; Ozturk, S.; Balkose, D.; Okur, S.; Ulku, S. Preparation and Characterization of Calcium Stearate Powders and Films Prepared by Precipitation and Langmuir- Blodgett Techniques. *Ind. Eng. Chem. Res.* **2010**, *49* (4), 1732−1736.
(66) Pukánszky, B.; Fekete, E. Adhesion and Surface Modification. In *Mineral Fillers in Thermoplastics I Raw Materials and Processing*; Springer Berlin Heidelberg, 1999; Vol. *139*, pp 109−153.
(67) Ricci, M.; Segura, J. J.; Erickson, B. W.; Fantner, G.; Stellacci, F.; Voïtchovsky, K. Growth and Dissolution of Calcite in the Presence of Adsorbed Stearic Acid. *Langmuir* **2015**, *31* (27), 7563−7571.
(68) Zhang, Z. X.; Dai, X. R.; Zou, L.; Wen, S. B.; Sinha, T. K.; Li, H. A Developed, Eco-Friendly, and Flexible Thermoplastic Elastomeric Foam from SEBS for Footwear Application. *eXPRESS Polym. Lett.* **2019**, *13* (11), 948−958.
(69) Huang, H.; Tian, M.; Yang, J.; Li, H.; Liang, W.; Zhang, L.; Li, X. Stearic Acid Surface Modifying Mg (OH) 2: Mechanism and Its Effect on Properties of Ethylene Vinyl Acetate/Mg (OH) 2 Composites. *J. Appl. Polym. Sci.* **2008**, *107* (5), 3325−3331.

https://doi.org/10.1021/acsomega.3c06186
ACS Omega 2024, 9, 11232−11242